Available online at www.sciencedirect.com
ScienceDirect
Earth and Planetary Science Letters 265 (2008) 535–545
EPSL
www.elsevier.com/locate/epsl

Ab initio study of the composition dependence of the pressure-induced spin crossover in perovskite $(Mg_{1-x},Fe_x)SiO_3$

Amelia Bengtson [a], Kristin Persson [b], Dane Morgan [c,*]

[a] *Materials Science Program, University of Wisconsin—Madison, 1509 University Ave, Room 201A MS&E, Madison, WI 53706, United States*
[b] *Department of Materials Science and Engineering, Massachusetts Institute of Technology, Room 13-5061, Cambridge, MA 02139, United States*
[c] *Department of Materials Science and Engineering, University of Wisconsin—Madison, 1509 University Ave, 244 MS&E, Madison, WI 53706, United States*

Received 29 June 2007; received in revised form 3 October 2007; accepted 21 October 2007
Available online 4 November 2007
Edited by: G.D. Price

Abstract

We present *ab initio* calculations of the zero-temperature iron high- to low-spin crossover in $(Mg_{1-x}Fe_x)SiO_3$ perovskite at pressures relevant to Earth's lower mantle. Equations of state are fit for a range of compositions and used to predict the Fe spin transition pressure and associated changes in volume and bulk modulus. We predict a dramatic decrease in transition pressure as Fe concentration increases. This trend is contrary to that seen in ferropericlase, and suggests the energetics for spin crossover is highly dependent on the structural environment of Fe. Both Local Density Approximation (LDA) and Generalized Gradient Approximation (GGA) exchange-correlation methods are used, and both methods reproduce the same compositional trends. However, GGA gives a significantly higher transition pressure than LDA. The spin transition is made easier by the decreasing spin-flip energy with pressure but is also driven by the change in volume from high to low spin. Volume trends show that high-spin Fe^{2+} is larger than Mg^{2+} even under pressure, but low-spin Fe^{2+} is smaller at ambient conditions and approximately the same size as Mg^{2+} under high pressure, indicating that low-spin Fe^{2+} is less compressible than high-spin Fe^{2+}. We find large changes between high- and low-spin in the slope of volume with Fe concentration. Although these changes are small in absolute magnitude for small Fe content, they are still important when measured per Fe and could be relevant for calculating partitioning coefficients in the lower mantle.

Keywords: spin transition; perovskite; lower mantle; *ab initio*; iron; low spin

1. Introduction

$(Mg,Fe,Al)(Si,Al)O_3$ perovskite (pv) and (Mg,Fe)O ferropericlase (fp) make up approximately 80% and 20% respectively of the volume of the lower mantle (Ito and Takahashi, 1987). A number of recent studies (see (Badro et al., 2003; Goncharov et al., 2006; Lin et al., 2007; Lin et al., 2006; Lin et al., 2005; Pasternak et al., 1997;

* Corresponding author. Tel.: +1 608 265 5879; fax: +1 608 262 8353.
E-mail addresses: akberta@wisc.edu (A. Bengtson), kpersson@mit.edu (K. Persson), ddmorgan@wisc.edu (D. Morgan).

0012-821X/$ - see front matter © 2007 Elsevier B.V. All rights reserved.
doi:10.1016/j.epsl.2007.10.049

Persson et al., 2006; Speziale et al., 2005) for fp and (Badro et al., 2005; Badro et al., 2004; Jackson et al., 2005; Li et al., 2004; Li et al., 2006; Li et al., 2005; Stackhouse et al., 2007; Zhang and Oganov, 2006) for pv) suggest that iron (Fe) undergoes a pressure-induced spin crossover in these phases, potentially impacting their equations-of-state, element partitioning, and mechanical, optical and transport properties. While substantial evidence exists for a high-spin (HS) to low-spin (LS) crossover under lower mantle pressures for Fe^{2+}in fp (Badro et al., 2003; Goncharov et al., 2006; Lin et al., 2007; Lin et al., 2006; Lin et al., 2005; Pasternak et al., 1997; Persson et al., 2006; Speziale et al., 2005), considerable uncertainty surrounds the spin behavior in pv (Badro et al., 2005; Badro et al., 2004; Jackson et al., 2005; Li et al., 2004; Li et al., 2006; Li et al., 2005; Stackhouse et al., 2007; Zhang and Oganov, 2006). This is due to the many variables that may affect the study of spin crossover: Fe site occupancy, Fe valence state, Fe concentration, Al content, possible intermediate spin states, and different experimental and computational techniques. However, in an attempt to understand and synthesize the existing knowledge on pv spin crossover, there are some trends that we can draw from the literature. In the following we will always be referring to low temperature results, where it seems that the crossover can be treated as a transition occurring in a relatively small range of pressures (the transition pressure will be denoted P_T, although it may be a range and not have a unique value). A comprehensive summary of the spin crossover measurements and calculations to date is given in Fig. 1. The first trend that we identify from this data is that in Al-free pv, Fe^{3+} has a lower P_T than Fe^{2+}. This effect of changing valence on P_T has been seen both experimentally (Badro et al., 2005; Badro et al., 2004; Jackson et al., 2005) and computationally (Li et al., 2005; Stackhouse et al., 2007; Zhang and Oganov, 2006). The second trend is that Al content significantly influences P_T, as experimental Al-free (Badro et al., 2005; Badro et al., 2004; Jackson et al., 2005) and Al-bearing (Li et al., 2004; Li et al., 2006) pv samples give a different P_T. Computationally, Fe^{3+} in Al-bearing pv has a higher P_T than in Al-free pv (Li et al., 2005; Stackhouse et al., 2007; Zhang and Oganov, 2006). A trend that is not clear from the literature is how P_T changes with Fe^{2+} concentration, which provides a central motivation for this paper.

At $x=1$ (pure $FeSiO_3$), previous calculations (Cohen et al., 1997; Stackhouse et al., 2006, 2007) found P_T values of 1000 GPa and 284 GPa, respectively, well outside the pressures expected in the lower mantle region. These results suggest that Fe^{2+} content dramatically drives up P_T in pv since both experimental and calculated results at lower Fe concentrations give much lower values for P_T. An increasing P_T with Fe^{2+} content would be consistent with the transition pressure trend seen in fp (Persson et al., 2006). However, the results of

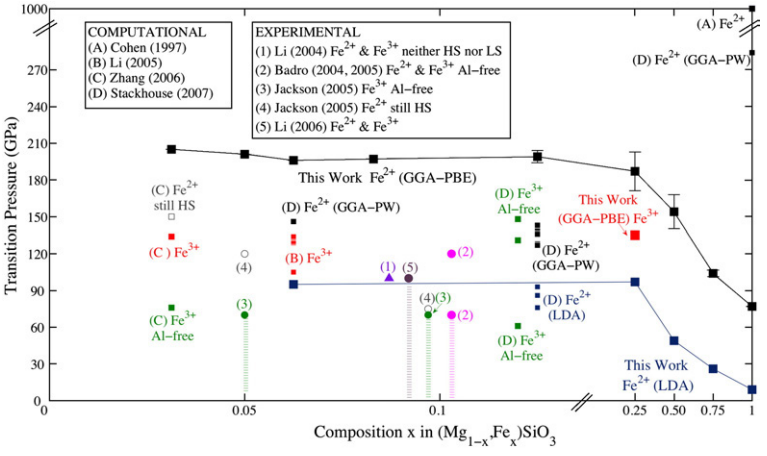

Fig. 1. Summary of this work and previously known high-spin (HS) to low-spin (LS) spin crossover pressures, P_T, in $(Mg_{1-x},Fe_x)SiO_3$, as a function of composition. Both experimental (circles) and computed (squares) data is included. For gradual crossovers, when data is available, the pressure range from the first sign of LS to complete LS is indicated by broken lines. The experimental crossover pressures are measured at room temperature. Iron valence states are indicated next to the reference. All Fe^{3+} samples include Al, except where indicated. Open symbols indicated all cases where up to the given pressure the system remains HS. The triangle at 100 GPa (Li et al., 2004) indicates that the experimental sample was in neither the HS nor LS state. Our work and Cohen et al. (1997); Li et al. (2005); Stackhouse et al. (2007); Zhang and Oganov (2006) are computational results. Data sets at $x=0.1$ (Badro et al., 2005; Badro et al., 2004; Li et al., 2004; Li et al., 2006) and $x=0.125$ (Stackhouse et al., 2007) have been shifted slightly in composition for clarity. P_T values for this work (GGA) for $x=0.125$, 0.25, 0.50, 0.75 Fe^{2+} are the mean of P_T's from the 2 SQS structures and the non-SQS 20-atom cell structures with error bars given as ±one standard deviation of the SQS and non-SQS P_T values.

this paper will show that in pv, P_T decreases as concentration of Fe^{2+} increases. We also explain why the present Fe end-member results are different than previous calculations (Cohen et al., 1997; Stackhouse et al., 2007).

We present results on the entire composition range from $x=0$ to $x=1$ in $(Mg_{1-x}Fe_x)SiO_3$ pv. The higher Fe contents are unlikely to be present in the lower mantle but significant uncertainty still exists regarding the amount of Fe present in pv at lower mantle conditions. Previous studies found concentration limits in pv of $x=0.15$ and $x=0.21$ for pv synthesized in multianvil apparatuses and diamond cells, respectively (as summarized in (Mao et al., 1997)). High-pressure and temperature experiments find stability limits of $x=0.28$ at 50 GPa in pv (Mao et al., 1997), and the pv phase diagram of Jeanloz and Thompson (1983) shows that $x=0.65$ is stable at 88 GPa and 1000 °C. Other studies predict that the Fe content in pv could be twice as much as in fp (Andrault, 2001). Recent experiments find $x=0.5$ is stable between 85–108 GPa and 1800–2330 K. In addition, high Fe content calculations (especially a fictive Fe end member) are of interest theoretically to calculate elastic properties (Mattern et al., 2005; Stackhouse et al., 2006) and phase stability (Caracas and Cohen, 2005).

Trends in volume with composition are important in calculations of the partitioning coefficient between pv and fp, which require knowledge of the equilibrium pv volume with respect to Fe concentration. The pv volume is currently estimated in the literature as $V_0(x)=V_0(x=0)+a(P)\times x$ where $V(x=0,P)$ is the equilibrium volume at pressure P for $MgSiO_3$, $a(P)$ is the pressure dependent coefficient, and x is the concentration of Fe (Andrault, 2001; Jackson, 1998; Jeanloz and Knittle, 1989; Kobayashi et al., 2005). We examine this volume relationship and suggest changes associated with spin crossover effects.

Finally, we consider trends in the spin crossover energetics with composition. Some previous energetic models of the spin crossover in the lower mantle have made assumptions about the bare energy required to change spin state ($\Delta E_{HS\text{-}LS}$) going to zero near the transition (Hofmeister, 2006; Sturhahn et al., 2005). However Persson et al. (2006) show that $\Delta E_{HS\text{-}LS}$ is not zero at the P_T for fp, and we show the same property holds for pv. We also show that $\Delta E_{HS\text{-}LS}$ has a strong composition dependence, which leads to the trends in P_T.

2. Computational method

Calculations were performed using density functional theory (DFT) and the projector-augmented plane-wave (PAW) method (Blochl, 1994; Kresse and Joubert, 1999), with the Vienna Ab-initio Simulation Package (VASP) (Kresse and Furthmuller, 1996). Exchange correlation was treated in both the Generalized Gradient Approximation (GGA), as parameterized in Perdew et al. (1996) (PBE), and the Local Density Approximation (LDA), as parameterized in Perdew and Zunger (1981) (CA). GGA tends to stabilize spin-polarized states over non-spin polarized compared to LDA (Stixrude et al., 1994), which will generally lead to higher spin transition pressures in GGA compared to LDA. In some cases DFT+U methods can provide a more accurate electronic structure for transition metal oxides with localized electrons, but the value of this approach for $(Mg,Fe)SiO_3$ is not clear and has not been explored here. In general we expect that adding a fixed U value to all phases with either GGA or LDA will drive up P_T (Persson et al., 2006). The PAW potentials were generated using the following electronic configurations: $2s^2\ 2p^4$ for Oxygen, $3\ p^6\ 3d^7\ 4s^1$ for Fe, $2p^6\ 3s^2$ for Mg, and $3s^2\ 3p^2$ for Si. Hard and soft oxygen PAW potentials supplied with the VASP package resulted in the same P_T to within 10 GPa for $FeSiO_3$. Calculations were done with energy cutoffs of 1050 eV and 441 eV for the hard and soft PAW potentials, respectively. Given the small differences found, the soft PAW potential was used in order to increase the speed of the calculations. The Brillouin zone was sampled by a Monkhorst–Pack k-point mesh of $3\times3\times2$ for the primitive cell of $MgSiO_3$ (d'Arco et al., 1993) and the Fourier space k-point density was kept as constant as possible for different cells. An energy cutoff of 441 eV was used. Total energy of the 20-atom primitive cell of $MgSiO_3$ was converged with respect to k-points and energy cutoff to better than 5 meV/atom. We estimate the errors in $MgSiO_3$ and $FeSiO_3$ for Equation of State (EOS) parameters K_0, E_0, V_0 and P_T are within 0.4%, 0.04%, 0.05%, 1% respectively with respect to energy cutoff and k-points.

The perovskite (pv) structure used is based on the experimentally determined $MgSiO_3$ orthorhombic cell, space group Pbnm (#62), containing 20 atoms in the primitive cell (d'Arco et al., 1993), four of which are metallic (Mg) sites. The alloy structures are created by substituting Fe^{2+} for a Mg atom on the A site, which is the site generally agreed upon for Fe^{2+} substitution (Vanpeteghem et al., 2006). Fe^{2+} is substituted for Mg to create concentrations of $x=0.25$, 0.5, 0.75 and 1. Within the 20-atom cell there is only one unique way to order the Fe^{2+} and Mg at each of these compositions, except at $x=0.50$ where the Fe^{2+} atoms were placed as far apart as possible (initial Fe–Fe distance of 4.665 Å). Below we discuss other arrangements at $x=0.50$. For Fe^{2+}

compositions of $x=0.125$, 0.083, 0.0625, 0.05, 0.03125 super cells of the original $MgSiO_3$ structure containing 40, 60, 80, 120, and 160 total atoms, respectively, were used.

The choice of Fe–Fe configurations can have a significant impact on the values of P_T (Li et al., 2005; Stackhouse et al., 2007). For low Fe^{2+} concentrations ($x<0.125$) there is only one Fe^{2+} per super cell in our calculations and this simulates the behavior of essentially isolated Fe. For higher Fe^{2+} concentrations ($x\geq 0.125$), since most experimental samples are reasonably approximated by a disordered solid solution, we designed special cells to mimic the disordered systems as closely as possible. The disordered system was modeled using 40-atom cell Special Quasirandom Structures (SQS) (Wei et al., 1990). SQS are small supercells with decorations chosen to mimic the local chemical order present in a truly random alloy. In this study, two different SQS are used to calculate EOS parameters and P_T for each of the Fe^{2+} compositions $x=0.125$, 0.25, 0.50 and 0.75 in addition to P_T calculations on the non-SQS $MgSiO_3$ 20-atom unit cell. The SQS structures are generated using the ATAT (van de Walle et al., 2002) toolkit to be as random as possible for Fe–Fe pairs within the first three nearest-neighbor shells. They are built as super cells of the 20-atom $MgSiO_3$ structure and are used to assess how far the results of the smaller 20-atom cells deviate from a disordered system.

All high-spin (HS) calculations were done as spin-polarized and ferromagnetic, and the low-spin (LS) calculations were done as non-spin polarized (0 magnetic moment). We found no significant difference in P_T when the LS enthalpies were calculated with a fixed spin set to zero, a varying spin optimized in the LS state, or as non-spin polarized. The use of ferromagnetic spin ordering is an approximation. The true ground state magnetic structure is likely to be composition dependent and have some antiferromagnetic character. In order to assess the possible impact of using a ferromagnetic spin ordering we have constructed an antiferromagnetic $FeSiO_3$ cell with perfect nearest-neighbor antiferromagnetic ordering on the approximately cubic Fe^{2+} sublattice. We find that the energy and P_T differ from the ferromagnetic values by 10 meV/Fe^{2+} and 5 GPa, respectively. Based on this energy difference, the magnetic ordering is likely to be paramagnetic for most compositions at room temperature and above. Since the impact of magnetism is likely to be largest at the $x=1$ composition the small changes we observe in $FeSiO_3$ associated with different magnetic ordering suggests that it is an excellent approximation for the properties discussed in this paper to treat all the compositions as ferromagnetic. To explore the intermediate spin (IS) state of Fe^{2+}, calculations were done for $x=0.25$ as described above with the spin state fixed to 2. Calculations at $x=0.25$ were also performed with Fe^{3+} by substituting an Fe atom for one of the symmetrically equivalent Mg atoms on the A site and Al for Si on the B site such that the Fe^{3+} and Al were nearest neighbors (the location of Fe^{3+} is pv samples is somewhat uncertain and this choice follows (Li et al., 2005)). The LS state of Fe^{3+} was fixed to a moment of 1.

Octahedral tilting plays an important role in the perovskite structure (Angel et al., 2005; Howard and Stokes, 2005; Lufaso and Woodward, 2004; Magyari-Kope et al., 2002; O'Keeffe et al., 1979). Therefore, in order to allow for internal distortions and octahedral tilting, each starting atomic position was perturbed by randomly adding or subtracting 0.01 Å along each Cartesian direction and no symmetry was enforced during the relaxations. Calculations were done with a grid of fixed volumes ranging from 200 $Å^3$ to 90 $Å^3$ for the 20-atom cell (and scaled appropriately for larger cells). The ions and cell shape were fully relaxed at each volume.

EOS parameters were calculated by fitting the energies as a function of volume over the pressure range $-10<P<200$ GPa using a least-squares fit to the Birch–Murnaghan third-order EOS (Birch, 1947) (additional fits using the Murnaghan (1944) and Vinet (Universal) (Fang, 1998; Vinet et al., 1986) EOS were also performed and any significant differences compared to the Birch–Murnaghan third-order fits are noted in the text.) The HS to LS transition pressure P_T was determined by the requirement of equal enthalpies (determined from the EOS) for both spin states.

3. Results

The third-order Birch–Murnaghan EOS parameters for calculated high-spin (HS) and low-spin (LS) perovskite (pv) fits for the VASP energies as a function of volume are given in Table 1 for both GGA and LDA results. These results do not include any of the SQS structures discussed above. For the SQS calculations K_0', E_0, and V_0 vary by less than 0.2% for HS and 0.4% for LS from the non-SQS structures. The SQS K_0 HS values are within 0.5% of the non-SQS structure, and LS are within 2%. A few general trends are obvious, particularly as a function of Fe^{2+} content, x, in $(Mg_{1-x}Fe_x)SiO_3$. For both HS and LS, the bulk moduli (K_0) increases with increasing x. Also, the equilibrium volume (V_0) increases (decreases) with increasing x for HS (LS). For all concentrations and spin states LDA gives larger K_0 and smaller V_0 than GGA, as

expected. V_0 decreases and K_0 increases from HS to LS, which is also to be expected, since LS Fe^{2+} is smaller than HS Fe^{2+} (Shannon, 1976), although the trends are not as evident for low Fe^{2+} concentrations. An assumption often made in calculating partitioning coefficients for low Fe^{2+} concentrations is that Fe^{2+} does not have an effect on K_0 (Andrault, 2001), which our results support for low x. However, for larger x values, K_0 increases with increasing Fe^{2+} content in both HS and LS. When the *ab initio* data was fit with the Murnaghan EOS or Vinet EOS (as opposed to the third-order Birch–Murnaghan EOS), similar trends were observed. E_0 and V_0 values changed by less than 0.005% and 0.25% respectively, and K_0 quantities were slightly higher for both Murnaghan and Vinet EOS by up to 4% (e.g. at $x=0$, $K_0=232$ GPa from the Vinet EOS).

Our results for $x=0$ agree as well as expected for density functional theory with the experimental results, where K_0 ranges between 247 and 272 GPa, K_0' ranges from 3.6–7, and V_0 is between 40.6–41.4 $Å^3$/f.u. (Akber-Knutson and Bukowinski, 2004; Caracas and Cohen, 2005; Mattern et al., 2005; Oganov et al., 2001). Our GGA results fall in the lowest part of the experimental K_0 range and are give somewhat expanded volumes compared to the experiments, which is typical for GGA. Our results also agree well with previous calculations, although one must take care to make comparisons to equivalent approaches. It particular, in order to correct for the overestimation of volume by GGA, a correction pressure is often applied, which we have not done in this paper. Comparisons of corrected and uncorrected values must be made appropriately. Also, comparisons should be made with the same EOS when possible to give the most direct assessment of the *ab initio* results. For $x=0$ our uncorrected K_0 and V_0 values match the uncorrected values of Oganov et al. (2001) very well, with volumes and bulk moduli agreeing within 0.3% (we used the same Vinet EOS as Oganov et al. for this comparison). Our V_0 is larger than that of Caracas and Cohen (2005) because their value has been adjusted by a pressure correction factor to match experimental values. The pressure correction factor required for our V_0 to match experiments is 9 GPa, similar to the correction pressure of 12 GPa used by Oganov et al. (2001). We choose to present all uncorrected values to avoid confusion and possible inconsistency at different Fe^{2+} compositions. For $x=0$, 0.50, and 1 our HS GGA and LDA K_0 values are within ±15 GPa of other computational values (summarized in (Caracas and Cohen, 2005)). Our LDA K_0, K_0', and V_0

Table 1
Third-order Birch–Murnaghan EOS parameters fitted for $-10<P<200$ GPa for HS and LS $(Mg_{1-x},Fe_x)SiO_3$ perovskite phases obtained by GGA and LDA calculations

x	GGA				LDA			
	K_0, GPa	K_0'	E_0, eV/f.u.	V_0, A^3/f.u.	K_0, GPa	K_0'	E_0, eV/f.u.	V_0, A^3/f.u.
High spin								
.0312	226	4.0648	−35.0785	42.198	–	–	–	–
.05	226	4.065	−35.1335	42.23	–	–	–	–
.0625	227	4.065	−35.1665	42.245	249	4.1409	−39.1345	40.206
.083	227	4.0654	−35.218	42.2775	–	–	–	–
.125	228	4.066	−35.318	42.307	–	–	–	–
.25	231	4.0712	−35.626	42.464	253	4.1526	−39.586	40.373
.50	234	4.0703	−36.2675	42.8405	262	4.1659	−40.2175	40.586
.75	242	4.0848	−36.909	43.03	271	4.1927	−40.8665	40.7225
1	248	4.0864	−37.569	43.3005	280	4.2086	−41.5335	40.887
1 AFM	243	4.0777	−37.562	43.3460	–	–	–	–
Low spin								
0	225	4.0636	−35.015	42.176	242	4.1655	−38.99	40.2245
.0312	226	4.0656	−35.0355	42.154	–	–	–	–
.05	226	4.0664	−35.066	42.1625	–	–	–	–
.0625	226	4.0674	−35.0825	42.158	226	4.4552	−39.108	40.43
.083	227	4.0685	−35.105	42.1525	–	–	–	–
.125	228	4.0685	−35.1515	42.1395	–	–	–	–
.25	231	4.0794	−35.295	42.1215	257	4.1583	−39.4	39.961
.50	242	4.1079	−35.711	41.8745	274	4.1888	−39.98	39.639
.75	255	4.1392	−36.1865	41.5175	294	4.2161	−40.644	39.189
1	271	4.1736	−36.7515	41.0625	312	4.3054	−41.42	38.7225

No SQS data is included.

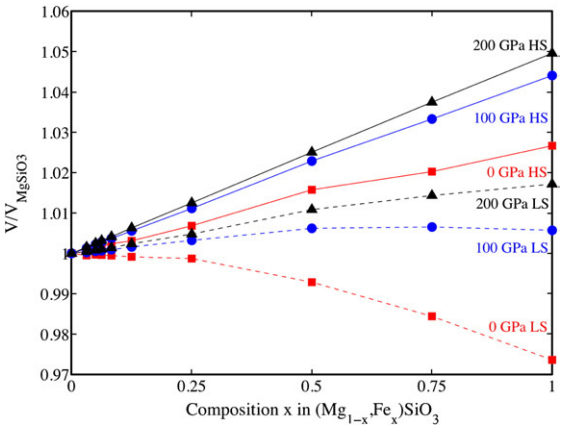

Fig. 2. Calculated HS (solid line) and LS (dashed line) $(Mg_{1-x},Fe_x)SiO_3$ volumes at $P=0$ (squares), 100 (circles) and 200 (triangles) GPa, as a ratio of the $MgSiO_3$ volume at each pressure, as a function of composition.

values give agreement to within ±15 GPa, ±0.1, and ±0.8 Å^3/f.u. respectively, with most other calculations (all comparisons made using the Vinet EOS) (Karki et al., 1997; Stixrude and Cohen, 1993; Wentzcovitch et al., 1995). However, for $x=0.5$ and 1 (Caracas and Cohen, 2005) obtain a larger volume than our results, suggesting a larger volume trend with concentration. At present we do not know the reason for this discrepancy.

Fig. 2 shows the HS and LS pv volumes (as a fraction of $MgSiO_3$ volume) as a function of Fe^{2+} content for several pressures. From Fig. 2 it is apparent that the volume difference between HS and LS, $\Delta V_{HS\text{-}LS}(P)$, increases with increasing Fe^{2+} content, as would be expected. In pv both HS and LS Fe^{2+} increase in size relative to Mg under pressure, suggesting that the Fe^{2+} is less compressible than Mg, consistent with the increased bulk modulus observed with Fe^{2+} doping. However, HS Fe^{2+} starts larger than Mg and keeps getting relatively larger, while LS Fe^{2+} starts smaller, and at relevant pressures of around 100 GPa is about equal in size to Mg. The increase in the volume of the HS states is quite close to linear with Fe^{2+} content, while the LS volumes show a clear convexity. The linear behavior is expected for a weakly interacting alloy system, whereas the convex behavior is consistent with strongly repulsive alloy systems, since the unlike-atom bonds tend to be longer than the like atom bonds. The volume trends are consistent with the energetics, which can be seen by viewing the system as a pseudo binary Mg–Fe alloy. The zero-pressure formation energy for $(Mg_{0.5}Fe_{0.5})SiO_3$ from $MgSiO_3$ and $FeSiO_3$ is about 20 meV/metal site for HS Fe^{2+}, but about 170 meV/metal site for LS Fe (these values change to 40 meV/metal site for HS Fe^{2+} and 210 meV/metal site for LS Fe at 100 GPa). Thus there is a dramatic increase in the repulsive interaction between Mg and Fe^{2+} (and associated tendency for phase separation and clustering) when Fe^{2+} goes LS. This unexpected change in the interactions as a function of spin state is under further investigation.

The HS to LS transition properties are given in Table 2 and Fig. 1. In Fig. 1, P_T values (GGA) for $x=0.125$, 0.25, 0.50, 0.75 Fe^{2+} are the mean of P_T's from the 2 SQS structures and the non-SQS 20-atom cell structures, with error bars given by one standard deviation. The relatively small error bars show that the non-SQS 20-atom cells give P_T values similar to the SQS cells. For low Fe^{2+} concentration P_T remains approximately constant and decreases as Fe^{2+} content increases. LDA gives lower P_T values than GGA, but reproduces the same qualitative trend. At $x=0.25$, Fe^{3+} shows a P_T of 135 GPa (lower than Fe^{2+} by about 60 to 100 GPa (Fig. 1)), which is in good agreement with the *ab initio* results of Li et al. (2005) and Zhang and Oganov (2006), although their results are at $x=0.0625$ and $x=0.03$, respectively. Table 2 also lists the change in volume (ΔV) at P_T as a function of x. We find the $\Delta V(P_T)$ trend with x increases non-linearly, which is due to the decrease of P_T with increasing x. All calculated transitions are sharp transitions from the HS to LS state and were done at 0 K. Temperature will stabilize the HS state and lead to a more continuous spin crossover (Lin et al., 2007; Sturhahn et al., 2005; Tsuchiya et al., 2006).

4. Discussion

4.1. Spin transition pressure dependence on composition

For low Fe^{2+} concentrations (i.e. low x in $(Mg_{1-x}Fe_x)SiO_3$) the Fe^{2+} GGA P_T is approximately independent of

Table 2
$(Mg_{1-x},Fe_x)SiO_3$ high- to low-spin transition pressures (P_T) for GGA and LDA from the EOS data in Table 1

x	GGA		LDA	
	P_T (GPa)	$\Delta V(P_T)$ Å^3/f.u.	P_T (GPa)	$\Delta V(P_T)$ Å^3/f.u.
.0312	193	0.0306	–	–
.05	190	0.0494	–	–
.0625	187	0.0616	96	0.1042
.083	192	0.0774	–	–
.125	202 (193,201)	0.1111	–	–
.25	201 (170,190)	0.2193	97	0.2483
.5	138 (162,162)	0.4771	49	0.648
.75	106 (101, 105)	0.8519	26	1.2147
1	77	1.37	9	1.9942

$\Delta V(P_T)$ is the change in volume from HS to LS at the transition pressure.
When available, P_T for 2 SQS structures are given in parentheses.

Fe^{2+} concentration and has a value of approximately 200 GPa, a trend that is reproduced with the LDA calculations, although with a lower P_T around 100 GPa. This lack of compositional dependence is to be expected since, for low x, Fe^{2+} is largely behaving as an isolated atom with respect to P_T. This result is similar to the lack of dependence of P_T on composition found for low Fe^{2+}content in ferropericlase (fp) by Tsuchiya et al. (2006).

Our P_T values are consistent with those in Zhang and Oganov, (2006), where Fe^{2+} was calculated to be HS up to 150 GPa (the highest pressure considered in that study). However, our P_T values are higher than Stackhouse et al. (2007) who found P_T at $x=0.125$ for Fe^{2+} to range from 127–143 GPa depending on Fe–Fe configuration, lower than our results and those of Zhang and Oganov (2006). The difference can be partly explained by the use of different parameterizations of the GGA. Stackhouse et al. used the Perdew–Wang parameterization of the GGA (GGA-PW) (Perdew et al., 1992, 1993), and we use the Perdew–Burke–Ernzerhof parameterization of the GGA (GGA-PBE) (Perdew et al., 1996). We find that switching to the GGA-PW for an $x=0.25$ SQS lowers P_T from 170 GPa to 137 GPa. Also, Stackhouse et al. (2007) used an 80 atom unit cell with the possibility of much closer Fe–Fe distances, whereas our cell at $x=0.125$ contained only 40 atoms. We found that using an 80-atom cell, with $x=0.125$ and a minimum Fe–Fe distance, lowered P_T from 202 GPa (40 atom cell, initial Fe–Fe distance of 4.979 Å) to 171 GPa (80-atom cell, initial Fe–Fe distance of 3.378 Å). Together, the exchange correlation and Fe^{2+} configuration differences can account for about a 60 GPa decrease in P_T between our work and that of Stackhouse et al., which is very close to what is observed. Therefore, large differences in P_T can be explained by changes in the parameterization of the GGA and the distance between the Fe–Fe neighbors within the cell.

For larger x, P_T decreases with increasing Fe^{2+} content, which was unexpected, since the opposite trend is observed in fp (with the rocksalt structure) (Persson et al., 2006) (Fig. 3). SQS calculations confirm that the lowering of P_T with higher Fe^{2+} content persists for approximately random disordered structures, so the trend is not an artifact of Fe–Fe ordering in smaller cells. However, all the cells we use are based on super cells of the $MgSiO_3$ structure. It is therefore possible that there are relaxations, particularly in the higher Fe^{2+} content cells (farther from the $MgSiO_3$ composition), that are not captured by our simulations and may impact our results. These could potentially be studied by more elaborate relaxation approaches, such as variable cell molecular dynamics (Wentzcovitch et al., 1993). The trend in P_T seen in fp is due to an effective chemical

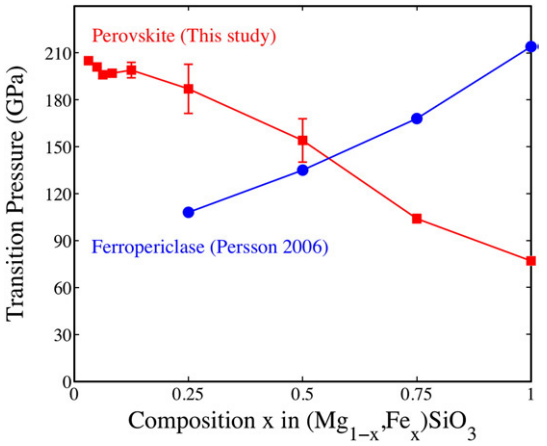

Fig. 3. Summary of transition pressures in perovskite and ferropericlase (rocksalt structure). Trends with composition are opposite depending on the material structure.

pressure from the Mg, which is discussed in detail in Persson et al. (2006). The relative atomic sizes that give rise to this chemical pressure also occur in pv, and should destabilize the HS Fe, driving P_T down with increasing Mg content. We therefore conclude that some other factor dominates over the effective chemical pressure to reverse the trend in P_T with composition.

We believe that the unexpected trend in pv P_T, opposite to that expected from chemical compression arguments and already seen in fp, is due to the additional distortions possible in the pv structure compared to fp. These distortions have a major effect in stabilizing the LS state. For example, the GGA P_T for $FeSiO_3$ (Fe^{2+} on the A site) is 77 GPa when the perturbed $MgSiO_3$ orthorhombic primitive cell is used as the starting structure, allowing extensive relaxations. However, if a 5-atom ideal cubic perovskite cell with full cubic symmetry is used, P_T is found to be 900 GPa. This dramatic dependence on structural relaxations occurs at other compositions as well. We propose that increasing stabilization of LS from the pv relaxations drives P_T down with increasing Fe^{2+} content.

The strong dependence of P_T on relaxations also explains some discrepancies with earlier results. Previous $FeSiO_3$ calculations found P_T to be 1000 GPa (Cohen et al., 1997) and 284 GPa (Stackhouse et al., 2006, 2007). The discrepancy between our results and these calculations is primarily due to the different structural relaxations allowed in each calculation. Our method, as outlined before, is to fully break all symmetry in the cell (by turning off the symmetry and adding small random perturbations to each atomic position) in order to allow full structural relaxation. If we calculate P_T for $FeSiO_3$ with the symmetry of the original

$MgSiO_3$ orthorhombic cell without adding the perturbations and maintaining the symmetry, we get a P_T value of 240 GPa, similar to P_T of 284 GPa found in Stackhouse et al. (2007). In Stackhouse et al. (2007), the enthalpies were extrapolated from 160 GPa, but in our study enthalpies were calculated to above 300 GPa, which, along with the use of a different GGA parameterization as mentioned previously, probably explains the remaining difference in P_T values. As mentioned above, if we constrain the calculations to the ideal cubic perovskite cell we find a P_T of 900 GPa, similar to the value found for the same cell in Cohen et al. (1997). Thus we have successfully replicated the other two previous computational P_T results on $FeSiO_3$ and show that allowing full structural relaxation dramatically lowers P_T. Stackhouse et al. (2006) also suggest that the LS $FeSiO_3$ structure is dynamically unstable. We do not find this instability, and propose that it is an additional result of working with a cell that is incompletely optimized with respect to the minimum energy atomic positions.

4.2. Spin transition pressure and intermediate spin and Fe valence

We saw no stable intermediate spin state (IS) at $x=0.25$ for Fe^{2+}, consistent with the results of Li et al. (2005) for Fe^{3+} and Stackhouse et al. (2007) for Fe^{2+}. However, in order to calculate an IS state, we fixed the spin state to 2 in our calculation. The actual IS state may have a magnetic moment slightly higher or lower than exactly 2, therefore further exploration of the other intermediate spin values is underway to confirm the absence of any predicted IS state.

Changing the Fe^{2+} species to Fe^{3+} on the A (Mg) site with the addition of Al on the B (Si) site in otherwise identical structures at $x=0.25$ lowers the GGA P_T from 196 GPa to 135 GPa (Fig. 1). This clearly establishes that, at least within density functional theory models, ferric and ferrous Fe have very different spin transition pressures, with ferric being much lower. Our Al-bearing Fe^{3+} P_T calculations are within the same range as the other Al-bearing computational results (Li et al., 2005; Zhang and Oganov, 2006), although their results are at $x=0.0625$ and $x=0.03$, respectively. The coupling of Fe^{2+} and Fe^{3+}, Fe^{3+} with no Al, and mixed and intermediate spin states are presently under investigation.

4.3. Volume dependence on composition

The volume trends in Fig. 2 provide useful information for calculation of partitioning coefficients. The volume relationship used for calculating partition coefficients is $V_0(x)=V_0(x=0)+a(P)\times x$, where x is the concentration of Fe, a is a fitting parameter, and P is the pressure. The values in this equation have previously been determined by fitting to pv data based on presumably HS Fe^{2+} (Andrault, 2001; Jackson, 1998; Jeanloz and Knittle, 1989; Kobayashi et al., 2005). Here we extend the fitting to explicitly include LS Fe. Because the lower mantle is thought to have low Fe^{2+}concentrations, we initially restrict our analysis to how $a(P)$ varies for small x. Fitting data in Table 1 $x\leq 0.25$ for HS Fe, our calculations gives $a(P=0)=4.7$, relatively close to the value of 6 found by fitting to experimental data in Andrault (2001). However, when Fe^{2+} is in the LS state (Fig. 2), a similar fit results in $a(P=0)=-0.8$. This demonstrates the dramatic impact of the change in spin state (although a smoother crossover due to temperature would ameliorate these effects). These calculations for $a(P)$ can easily be extended to arbitrary pressures using our equations of state. Fits are given for $x\leq 0.25$ and $x\geq 0.25$ in order to best describe the behavior in the dilute Fe and Fe-rich regions. Fitting to data for $x\leq 0.25$ at $P=0$, 25, 50, 100, 150, and 200 GPa gives $a(P)=-6.46\times10^{-9}\ P^4+3.37\times10^{-6}\ P^3-6.58\times10^{-4}\ P^2+6.36\times10^{-2}\ P-0.80$ for LS Fe^{2+} and $a(P)=-5\times10^{-9}\ P^4+2.70\times10^{-6}\ P^3-5.02\times10^{-4}\ P^2+3.98\times10^{-2}\ P+4.66$ for HS Fe^{2+}. Fitting for the same pressures and for $x\geq 0.25$ gives $a(P)=-1.31\times10^{-8}\ P^4+6.90\times10^{-6}\ P^3-1.38\times10^{-3}\ P^2+1.42\times10^{-1}\ P-5.64$ for LS Fe^{2+} and $a(P)=-5.51\times10^{-9}\ P^4+2.83\times10^{-6}\ P^3-5.33\times10^{-4}\ P^2+4.39\times10^{-2}\ P+4.32$ for HS Fe^{2+}.

Note that for mixed spin states, as is expected at higher temperatures, one can approximate the volume trends by interpolating between these expressions.

4.4. Energetics of the spin transition

Assuming we are at zero Kelvin, the spin transition will occur when the enthalpy of the HS state exceeds that of the LS state. At the transition the difference in enthalpy $\Delta H_{HS\text{-}LS}(P)=\Delta E_{HS\text{-}LS}(P)+P\Delta V_{HS\text{-}LS}(P)$ is zero. In Fig. 4, both enthalpy terms for GGA are plotted at 0 GPa, 100 GPa, and 200 GPa. We find that $\Delta E_{HS\text{-}LS}$ is not zero at P_T (as is sometimes assumed, e.g. in (Hofmeister, 2006) and (Sturhahn et al., 2005)), and that the spin transition occurs when a significant $P\Delta V_{HS\text{-}LS}$ term balances the $\Delta E_{HS\text{-}LS}$ term at P_T. Since $P\Delta V_{HS\text{-}LS}$ changes most under compression it is the change in volume that largely drives the transition. As a function of pressure the change in $P\Delta V_{HS\text{-}LS}$ is larger than $\Delta E_{HS\text{-}LS}$, but not as large as the difference is in the fp structure (Persson et al., 2006). As a function of Fe^{2+}

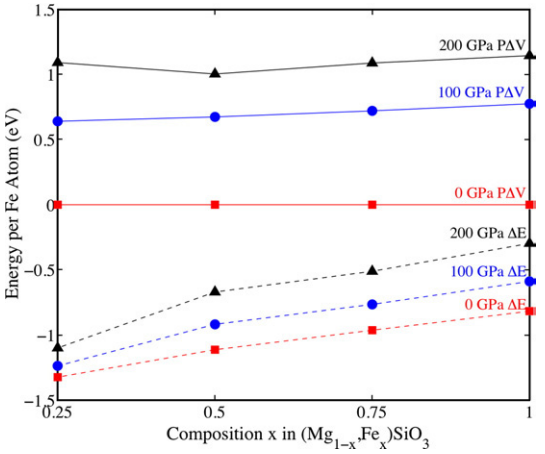

Fig. 4. Calculated $\Delta E_{\text{HS-LS}}(P)$ (dashed line) and $P\Delta V_{\text{HS-LS}}(P)$ (solid line) terms as a function of composition, at $P=0$ (squares), 100 (circles), and 200 (triangles) GPa.

content, the magnitude of $\Delta E_{\text{HS-LS}}$ decreases but $P\Delta V_{\text{HS-LS}}$ remains nearly constant. The trend in $\Delta E_{\text{HS-LS}}$ stabilizes the LS state and leads to the decreasing values of P_T with increasing Fe^{2+} content. The higher Fe^{2+} content may allow for more energetically favorable distortions which stabilize the LS state, as suggested above. Other possible causes, e.g., changes in the electronic structure, could not be conclusively identified in this study. The behavior of $\Delta E_{\text{HS-LS}}$ is very different in pv than fp. In fp $\Delta E_{\text{HS-LS}}$ increases as Fe^{2+} content increases, stabilizing the HS state (Persson et al., 2006). These results suggest that for both pv and fp a major contribution to the driving force for pressure-induced transitions is the volume difference between HS and LS phases, even more than the reduction of the fixed volume spin-flip energy. However, opposite trends between pv and fp in the spin-flip energy give opposite trends in P_T with Fe^{2+} content.

5. Conclusions

The results presented have a number of implications for understanding Fe^{2+} spin behavior in $(Mg_{1-x},Fe_x)SiO_3$. While P_T in Fe^{2+} is relatively constant at low x it decreases as x increases. We predict a P_T for $x=1$ that is much smaller than previous calculations (Cohen et al., 1997; Stackhouse et al., 2007), and suggest that Fe^{2+} rich pv could easily be LS within the lower mantle region. These trends are counter those expected from chemical pressure arguments and seen in fp, which we propose is due to relaxations in the pv structure. Similar to fp, we find that in pv LS Fe^{2+} is significantly smaller than HS Fe, but that LS Fe^{2+} and Mg become similar in size at higher pressures. The LDA results indicate the possibility of LS Fe^{2+} in pv in the lower mantle over the entire composition range, however GGA results indicate that only pv with $x>0.25$ will have LS Fe^{2+} in the lower mantle. While a reliable spin crossover value is difficult to pin down from this data, it is clear that experiments on higher Fe compositions at lower mantle conditions should particularly consider the possibility of LS Fe within their samples. The gradual spin crossover seen in experiments (Badro et al., 2005; Badro et al., 2004; Jackson et al., 2005; Li et al., 2004; Li et al., 2006) could be explained either by the Fe^{3+} going LS before Fe^{2+} (as indicated by our results) or by different local clusters of Fe going LS at different pressures. Also, our calculations do not yet rule out the possibility of an intermediate spin state.

Future analysis that considers trends in volume and elastic properties with Fe^{2+} content must now consider the possibility of LS Fe^{2+}. To help with such analysis we provide equation of state data for HS and LS Fe^{2+} for a range of compositions, including pressure dependent fits to the volume changes associated with dilute HS and LS Fe^{2+}. Temperature will stabilize HS and drive up P_T at a given composition, and these effects are currently under investigation.

Computationally, we have shown that LDA gives a P_T lower than GGA by a shift of ~70–90 GPa, suggesting that further study of optimal exchange-correlation functions, and possibly investigation of correlated methods such as LDA+U, needs to be performed for more quantitative predictions of P_T. We have also shown that using the PW parameterization of GGA instead of PBE lowers P_T by over 30 GPa, and close Fe–Fe distances can lower P_T by over 30 GPa as well. We predict that Fe^{3+} exhibits a significantly lower P_T than Fe^{2+} although further study of Fe^{2+}–Fe^{3+} interactions, site occupations, and intermediate spin states is needed. Our results also show that the consideration of pressure–volume terms in the enthalpy is equally or more important in determining the transition pressure as the bare energy required to change the spin state at constant volume.

Acknowledgements

Financial support from Wisconsin Alumni Research Foundation (WARF) and MIT Institute for Soldier Nanotechnologies, Grant DAAD19-02-D-0002 are gratefully acknowledged. We are grateful to G. Ceder, J. Li, J. Lin, J. Badro, L. Li, and S. Stackhouse for support and helpful discussions.

References

Akber-Knutson, S., Bukowinski, M.S.T., 2004. The energetics of aluminum solubility into $MgSiO_3$ perovskite at lower mantle conditions. Earth Planet. Sci. Lett. 220 (3–4), 317–330.

Andrault, D., 2001. Evaluation of (Mg,Fe) partitioning between silicate perovskite and magnesiowustite up to 120 GPa and 2300 K. J. Geophys. Res. B 106 (B2), 2079–2087.

Angel, R.J., Zhao, J., Ross, N.L., 2005. General rules for predicting phase transitions in perovskites due to octahedral tilting. Phys. Rev. Lett. 95 (2), 025503.

Badro, J., Fiquet, G., Guyot, F., 2005. Thermochemical state of the lower mantle: new insights from mineral physics. Earth's Deep Mantle: Structure, Composition, and Evolution. R.D. van der Hilst, J.D. Bass, J. Matas, J. Trampert. American Geophysical Union 160, 241–260.

Badro, J., Fiquet, G., Guyot, F., Rueff, J.P., Struzhkin, V.V., Vanko, G., Monaco, G., 2003. Iron partitioning in Earth's mantle: toward a deep lower mantle discontinuity. Science 300 (5620), 789–791.

Badro, J., Rueff, J.P., Vanko, G., Monaco, G., Fiquet, G., Guyot, F., 2004. Electronic transitions in perovskite: possible nonconvecting layers in the lower mantle. Science 305 (5682), 383–386.

Birch, F., 1947. Finite elastic strain of cubic crystals. Phys. Rev. 71 (11), 809–824.

Blochl, P.E., 1994. Projector augmented-wave method. Phys. Rev. B 50 (24), 17953–17979.

Caracas, R., Cohen, R.E., 2005. Effect of chemistry on the stability and elasticity of the perovskite and post-perovskite phases in the $MgSiO_3$–$FeSiO_3$–Al_2O_3 system and implications for the lowermost mantle. Geophys. Res. Lett. 32, L16310.

Cohen, R.E., Mazin, I.I., Isaak, D.G., 1997. Magnetic collapse in transition metal oxides at high pressure: implications for the Earth. Science 275 (5300), 654–657.

d'Arco, P., Sandrone, G., Dovesi, R., Orlando, R., Saunders, V.R., 1993. A quantum mechanical study of the perovskite structure type of $MgSiO_3$. Phys. Chem. Minerals 20 (6), 407–414.

Fang, Z.H., 1998. Extension of the universal equation of state for solids in high-pressure phases. Phys. Rev. B 58 (1), 20–22.

Goncharov, A.F., Struzhkin, V.V., Jacobsen, S.D., 2006. Reduced radiative conductivity of low-spin (Mg,Fe)O in the lower mantle. Science 312 (5777), 1205–1208.

Hofmeister, A.M., 2006. Is low-spin Fe2+present in Earth's mantle? Earth Planet. Sci. Lett. 243 (1–2), 44–52.

Howard, C.J., Stokes, H.T., 2005. Structures and phase transitions in perovskites — a group-theoretical approach. Acta Cryst. A 61, 93–111.

Ito, E., Takahashi, E., 1987. Ultrahigh-pressure phase transformations and the constitution of the deep mantle. *High-Pressure Research in Mineral Physics*, Tokyo. Terra Scientific Pub. Co., Washington, D.C., pp. 221–229. American Geophysical Union, 1987.

Jackson, I., 1998. Elasticity, composition and temperature of the Earth's lower mantle: a reappraisal. Geophys. J. Int. 134 (1), 291–311.

Jackson, J.M., Sturhahn, W., Shen, G.Y., Zhao, J.Y., Hu, M.Y., Errandonea, D., Bass, J.D., Fei, Y.W., 2005. A synchrotron Mossbauer spectroscopy study of $(Mg,Fe)SiO_3$ perovskite up to 120 GPa. Am. Miner. 90 (1), 199–205.

Jeanloz, R., Knittle, E., 1989. Density and composition of the lower mantle. Phil. Trans. R. Soc. A 328 (1599), 377–389.

Jeanloz, R., Thompson, A.B., 1983. Phase-transitions and mantle discontinuities. Rev. Geophys. 21 (1), 51–74.

Karki, B.B., Stixrude, L., Clark, S.J., Warren, M.C., Ackland, G.J., Crain, J., 1997. Elastic properties of orthorhombic $MgSiO_3$ perovskite at lower mantle pressures. Am. Miner. 82 (5–6), 635–638.

Kobayashi, Y., Kondo, T., Ohtani, E., Hirao, N., Miyajima, N., Yagi, T., Nagase, T., Kikegawa, T., 2005. Fe–Mg partitioning between $(Mg, Fe)SiO_3$ post-perovskite, perovskite, and magnesiowustite in the Earth's lower mantle. Geophys. Res. Lett. 32, L19301.

Kresse, G., Furthmuller, J., 1996. Efficiency of ab-initio total energy calculations for metals and semiconductors using a plane-wave basis set. Comp. Mater. Sci. 6 (1), 15–50.

Kresse, G., Joubert, D., 1999. From ultrasoft pseudopotentials to the projector augmented-wave method. Phys. Rev. B 59 (3), 1758–1775.

Li, J., Struzhkin, V.V., Mao, H.K., Shu, J.F., Hemley, R.J., Fei, Y.W., Mysen, B., Dera, P., Prakapenka, V., Shen, G.Y., 2004. Electronic spin state of iron in lower mantle perovskite. Proc. Natl. Acad. Sci. U. S. A. 101 (39), 14027–14030.

Li, J., Sturhahn, W., Jackson, J.M., Struzhkin, V.V., Lin, J.F., Zhao, J., Mao, H.K., Shen, G.Y., 2006. Pressure effect on the electronic structure of iron in (Mg,Fe)(Si,Al)O3 perovskite: a combined synchrotron Mössbauer and X-ray emission spectroscopy study up to 100 GPa. Phys. Chem. Min. 33 (8–9), 575–585.

Li, L., Brodholt, J.P., Stackhouse, S., Weidner, D.J., Alfredsson, M., Price, G.D., 2005. Electronic spin state of ferric iron in Al-bearing perovskite in the lower mantle. Geophys. Res. Lett. 32, L17307.

Lin, J.-F., Vankó, G., Jacobsen, S.D., Iota, V., Struzhkin, V.V., Prakapenka, V.B., Kuznetsov, A., Yoo, C.-S., 2007. Spin transition zone in Earth's lower mantle. Science 317, 1740–1743.

Lin, J.F., Gavriliuk, A.G., Struzhkin, V.V., Jacobsen, S.D., Sturhahn, W., Hu, M.Y., Chow, P., Yoo, C.S., 2006. Pressure-induced electronic spin transition of iron in magnesiowustite-(Mg,Fe)O. Phys. Rev. B 73, 113107.

Lin, J.F., Struzhkin, V.V., Jacobsen, S.D., Hu, M.Y., Chow, P., Kung, J., Liu, H.Z., Mao, H.K., Hemley, R.J., 2005. Spin transition of iron in magnesiowustite in the Earth's lower mantle. Nature 436 (7049), 377–380.

Lufaso, M.W., Woodward, P.M., 2004. Jahn–Teller distortions, cation ordering and octahedral tilting in perovskites. Acta Cryst. B 60, 10–20.

Magyari-Kope, B., Vitos, L., Grimvall, G., Johansson, B., Kollar, J., 2002. Low-temperature crystal structure of $CaSiO_3$ perovskite: an ab initio total energy study. Phys. Rev. B 65, 193107.

Mao, H.K., Shen, G.Y., Hemley, R.J., 1997. Multivariable dependence of Fe–Mg partitioning in the lower mantle. Science 278 (5346), 2098–2100.

Mattern, E., Matas, J., Ricard, Y., Bass, J., 2005. Lower mantle composition and temperature from mineral physics and thermodynamic modelling. Geophys. J. Int. 160 (3), 973–990.

Murnaghan, F.D., 1944. The compressibility of media under extreme pressures. Proc. Natl. Acad. Sci. 30, 244–247.

O'Keeffe, M., Hyde, B., Bovin, J., 1979. Contribution to the crystal chemistry of orthorhombic perovskites: $MgSiO_3$ and $NaMgF_3$. Phys. Chem. Minerals 4 (4), 299–305.

Oganov, A.R., Brodholt, J.P., Price, G.D., 2001. Ab initio elasticity and thermal equation of state of $MgSiO_3$ perovskite. Earth Planet. Sci. Lett. 184 (3–4), 555–560.

Pasternak, M.P., Taylor, R.D., Jeanloz, R., Li, X., Nguyen, J.H., McCammon, C.A., 1997. High pressure collapse of magnetism in Fe0.94O: Mossbauer spectroscopy beyond 100 GPa. Phys. Rev. Lett. 79 (25), 5046–5049.

Perdew, J.P., Burke, K., Ernzerhof, M., 1996. Generalized gradient approximation made simple. Phys. Rev. Lett. 77 (18), 3865–3868.

Perdew, J.P., Chevary, J.A., Vosko, S.H., Jackson, K.A., Pederson, M.R., Singh, D.J., Fiolhais, C., 1992. Atoms, molecules, solids, and

surfaces — applications of the generalized gradient approximation for exchange and correlation. Phys. Rev. B 46 (11), 6671–6687.

Perdew, J.P., Chevary, J.A., Vosko, S.H., Jackson, K.A., Pederson, M.R., Singh, D.J., Fiolhais, C., 1993. Erratum: Atoms, molecules, solids, and surfaces: applications of the generalized gradient approximation for exchange and correlation. Phys. Rev. B 48 (7), 4978–4978.

Perdew, J.P., Zunger, A., 1981. Self-interaction correction to density-functional approximations for many-electron systems. Phys. Rev. B 23 (10), 5048–5079.

Persson, K., Bengtson, A., Ceder, G., Morgan, D., 2006. Ab initio study of the composition dependence of the pressure-induced spin transition in the $(Mg_{1-x},Fe_{-x})O$ system. Geophys. Res. Lett. 33 (16), L16306.

Shannon, R.D., 1976. Revised effective ionic-radii and systematic studies of interatomic distances in halides and chalcogenides. Acta Cryst. A 32 (SEP1), 751–767.

Speziale, S., Milner, A., Lee, V.E., Clark, S.M., Pasternak, M.P., Jeanloz, R., 2005. Iron spin transition in Earth's mantle. Proc. Natl. Acad. Sci. U. S. A. 102 (50), 17918–17922.

Stackhouse, S., Brodholt, J.P., Price, G.D., 2006. Elastic anisotropy of $FeSiO_3$ end-members of the perovskite and post-perovskite phases. Geophys. Res. Lett. 33 (1), L01304.

Stackhouse, S., Brodholt, J.P., Price, G.D., 2007. Electronic spin transitions in iron-bearing $MgSiO_3$ perovskite. Earth Planet. Sci. Lett. 253 (1–2), 282–290.

Stixrude, L., Cohen, R.E., 1993. Stability of orthorhombic $MgSiO_3$ perovskite in the Earth's lower mantle. Nature 364 (6438), 613–616.

Stixrude, L., Cohen, R.E., Singh, D.J., 1994. Iron at high-pressure-linearized-augmented-plane-wave computations in the generalized-gradient approximation. Phys. Rev. B 50 (9), 6442–6445.

Sturhahn, W., Jackson, J.M., Lin, J.F., 2005. The spin state of iron in minerals of Earth's lower mantle. Geophys. Res. Lett. 32 (12), L12307.

Tsuchiya, T., Wentzcovitch, R.M., da Silva, C.R.S., de Gironcoli, S., 2006. Spin transition in magnesiowustite in earth's lower mantle. Phys. Rev. Lett. 96 (19), 198501.

van de Walle, A., Asta, M., Ceder, G., 2002. The Alloy Theoretic Automated Toolkit: a user guide. Calphad-Computer Coupling of Phase Diagrams and Thermochemistry 26 (4), 539–553.

Vanpeteghem, C.B., Angel, R.J., Ross, N.L., Jacobsen, S.D., Dobson, D.P., Litasov, K.D., Ohtani, E., 2006. Al, Fe substitution in the $MgSiO_3$ perovskite structure: a single-crystal X-ray diffraction study. Phys. Earth Planet. Inter. 155 (1–2), 96–103.

Vinet, P., Ferrante, J., Smith, J.R., Rose, J.H., 1986. A universal equation of state for solids. J Phys C Solid State Phys 19 (20), L467–L473.

Wei, S.H., Ferreira, L.G., Bernard, J.E., Zunger, A., 1990. Electronic-properties of random alloys — special quasirandom structures. Phys. Rev. B 42 (15), 9622–9649.

Wentzcovitch, R.M., Martins, J.L., Price, G.D., 1993. Abinitio molecular-dynamics with variable cell-shape — application to $MgSiO_3$. Phys. Rev. Lett. 70 (25), 3947–3950.

Wentzcovitch, R.M., Ross, N.L., Price, G.D., 1995. Ab-initio study of $MgSiO_3$ and $CaSiO_3$ perovskites at lower-mantle pressures. Phys. Earth Planet Int. 90 (1–2), 101–112.

Zhang, F., Oganov, A.R., 2006. Valence state and spin transitions of iron in Earth's mantle silicates. Earth Planet. Sci. Lett. 249 (3–4), 436–443.